Inner–Outer Loop Control for Quadrotor UAVs With Input and State Constraints

Ning Cao and Alan F. Lynch, *Member, IEEE*

***Abstract*— The constrained control of unmanned aerial vehicles (UAVs) is a challenging task due to their nonlinear and underactuacted dynamics. This brief focuses on the position control of a quadrotor UAV with state and input constraints using an inner–outer loop control structure. The outer loop generates a saturated thrust, and the reference roll and pitch angles, while the inner loop is designed to follow these reference angles using a traditional PID controller. Assuming perfect inner loop tracking, the outer loop nested saturation controller guarantees global asymptotic stability for output regulation and tracking. The effect of nonideal inner loop tracking on closed-loop stability is analyzed. The proposed method is experimentally validated on an indoor quadrotor platform.**

***Index Terms*— Flight testing, inner–outer loop control structure, input and state constraints, nonlinear control, unmanned aerial vehicles (UAVs).**

I. Introduction

UNMANNED aerial vehicles (UAVs) are receiving increasing interest from industry and academia due to their suitability for dull, dirty, and dangerous missions, such as infrastructure inspection and surveillance. Nonlinear motion control of rotary-wing UAVs has received significant attention to date [1]–[3]. Some works, such as [4]–[7], focus on traditional helicopter UAVs whereas the research on quadrotors has emerged more recently [7]–[12]. Helicopter and quadrotor UAVs have the same dynamics if we ignore differences in their thrust and torque input models. Most field tested autopilots use an inner–outer loop or a cascade control structure [2], [13]. The idea of separating the control into two (or more) cascaded loops is seen in many applications, such as electric motor drives and static synchronous compensators for power quality control [14]. The benefits of a two (or more) loop structure include simplicity of implementation, ease of tuning, and satisfaction on input or state constraints. For UAVs, the outer loop stabilizes translational variables, i.e., position and linear velocity, and generates a reference signal fed to the inner loop. Separating the control into simpler translational and rotational designs is important for reliable practical implementation [13], [15]–[18]. The indoor and outdoor UAVs developed at the Applied Nonlinear Control Laboratory (ANCL), University of Alberta, have been experimentally tested using an inner-outer loop control structure [12], [19], [20].

Manuscript received March 30, 2015; revised September 11, 2015; accepted November 19, 2015. Date of publication December 30, 2015; date of current version August 4, 2016. Manuscript received in final form December 1, 2015. Recommended by Associate Editor A. Tayebi.

The authors are with the Department of Electrical and Computer Engineering, University of Alberta, Edmonton, AB T6G 1H9, Canada (e-mail: ncao@ualberta.ca; alan.lynch@ualberta.ca).

This paper has supplementary downloadable material available at http://ieeexplore.ieee.org., provided by the author.

Color versions of one or more of the figures in this paper are available online at http://ieeexplore.ieee.org.

Digital Object Identifier 10.1109/TCST.2015.2505642

Due to physical constraints of actuators, e.g., UAV rotor speed, many researchers study motion control with input saturation [21]. In addition, constraints on states should also be considered for practical reasons [22]. For example, it is necessary to constrain attitude to a safe range to avoid undesirable UAV configurations (e.g., an inverted aircraft). Constraints on attitude are also useful for visual servoing applications where an on-board camera is used to provide feedback for motion control [8], [12]. Here, attitude must be limited to ensure the visual target remains in the camera's field of view. The inner–outer loop control structure is useful for limiting attitude, since the inner loop references can be saturated [13]. Examples of work on input constraints include [23], which uses nested saturation [24] and an approximate linearized model to account for thrust and torque limits. Metni and Hamel [25] consider a visual servoing application and incorporate orientation limits using nested saturation and the angle between the z-axes of the inertial and body frames. A cascade framework using the rotation matrix is in [18], which includes bounds on thrust.

In this brief, we design an inner loop using a conventional PID controller based on a rotational model involving Euler angles. This control tracks the reference roll and pitch calculated in the outer loop and a given yaw trajectory. A commonly used PID structure based on Euler angles is relatively easy to implement and tune on-board, and is robust to disturbances [11], [26]–[28]. Other parameterizations of the rotation matrix have been used to design the inner loop. For example, rotation matrices [29] or quaternions [9] avoid Euler angle singularities and provide almost global stabilization results. However, we use Euler angles in this brief given their improved track record for performance and ease of use. The proposed outer loop generates a saturated thrust and bounded reference for roll and pitch, which globally asymptotically stabilize the translational dynamics. We also analyze the performance of the entire inner–outer closed-loop and conclude asymptotic stability. The performance of the proposed method is experimentally validated on an indoor quadrotor test stand.

Unlike many existing approaches, we use the body frame representation of the translational dynamics. This provides two advantages. First, it allows for independent bounds for roll and pitch. In the inertial frame, the velocity dynamics leads to roll and pitch references which depend on yaw explicitly. This makes it impossible to individually bound roll and pitch. Second, an advantage of using the body frame is that it is similar to the camera frame used in image-based visual servoing [8]. Since both frames are rigidly attached to the UAV, the resulting dynamics has a similar structure and the proposed method can be applied to visual servoing. In a visual servoing application it is important to

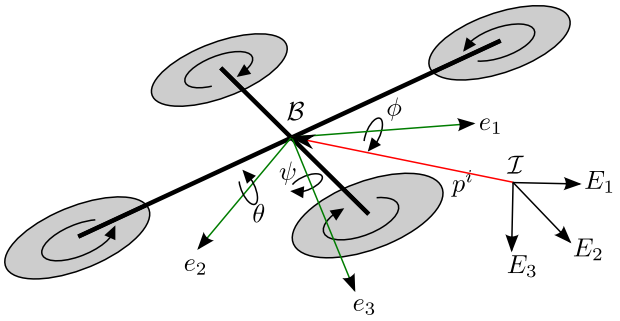

Fig. 1. Quadrotor modeling.

individually control roll and pitch since the image plane is not square.

This brief is organized as follows. The dynamics is given in Section II. In Section III, the inner and outer loop controllers are proposed and the global asymptotic stability of the outer loop is proved with perfect inner loop tracking. Then, the analysis of nonideal inner loop performance on closed-loop stability is provided. The experimental and simulation results are given in Section IV.

II. Quadrotor Modeling

In this section, we recall a relatively simple dynamics of a quadrotor [7]. Fig. 1 shows the two reference frames used. An inertial frame $\mathcal{I}$ is stationary with respect to the earth and has an orthonormal basis $\{E_1, E_2, E_3\}$ with E_3 pointing down. The body frame $\mathcal{B}$ is fixed to the center of mass and has orthonormal basis $\{e_1, e_2, e_3\}$. The vector e_3 points down. The rigid body dynamics expressed in $\mathcal{B}$ is

$$\dot{p}^b = -\mathrm{sk}(\omega^b)\, p^b + v^b \tag{1a}$$

$$\dot{v}^b = -\mathrm{sk}(\omega^b) v^b + g R^T E_3 - \frac{T}{m} e_3 \tag{1b}$$

$$\dot{\eta} = W(\eta)\omega^b \tag{1c}$$

$$J\dot{\omega}^b = -\omega^b \times J\omega^b + \tau^b \tag{1d}$$

where p^b is the position expressed in $\mathcal{B}$, v^b is the velocity expressed in $\mathcal{B}$, m is the vehicle mass, g is the gravity constant, J is the inertia matrix, R is a rotation matrix, and ω^b is the angular velocity expressed in $\mathcal{B}$. The operator $\mathrm{sk} : \mathbb{R}^3 \to \mathbb{R}^{3\times 3}$ is defined as $\mathrm{sk}(x)y = x \times y$, where $x, y \in \mathbb{R}^3$. The external force expressed in $\mathcal{B}$ is $-Te_3$, $T > 0$. Here, we have assumed that this force results from the four propellers and it acts in the e_3 direction (i.e., no blade flapping). The applied torque due to the propellers expressed in $\mathcal{B}$ is τ^b. We treat T and τ^b as control inputs. We have parametrized R with ZYX Euler angles $\eta = [\phi, \theta, \psi]^T$. Hence

$$R(\eta) = \begin{bmatrix} c_\psi c_\theta & -s_\psi c_\phi + c_\psi s_\theta s_\phi & s_\phi s_\psi + c_\phi s_\theta c_\psi \\ s_\psi c_\theta & c_\psi c_\phi + s_\psi s_\theta s_\phi & -s_\phi c_\psi + c_\phi s_\theta s_\psi \\ -s_\theta & c_\theta s_\phi & c_\theta c_\phi \end{bmatrix}$$

$$W(\eta) = \begin{bmatrix} 1 & s_\phi t_\theta & c_\phi t_\theta \\ 0 & c_\phi & -s_\phi \\ 0 & s_\phi / c_\theta & c_\phi / c_\theta \end{bmatrix}$$

where $s_\phi = \sin\phi$, $c_\phi = \cos\phi$, $t_\theta = \tan\theta$, and ϕ, θ, and ψ denote roll, pitch, and yaw, respectively. The position and velocity vectors can be expressed in $\mathcal{B}$ or $\mathcal{I}$ with $p^i = Rp^b$ and $v^i = Rv^b$.

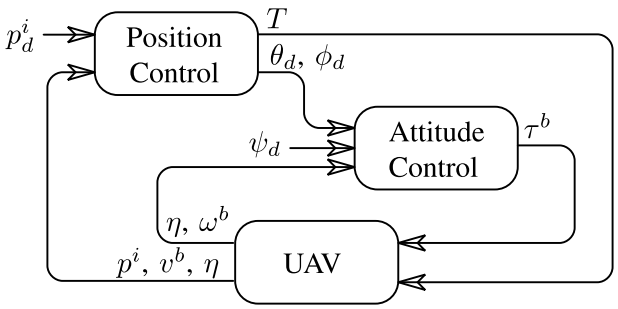

Fig. 2. Inner–outer loop controller structure.

The reason for expressing the translational dynamics in $\mathcal{B}$ is that it prevents ψ from explicitly appearing in (1b), and this allows us to bound ϕ and θ independently. In particular, we consider the velocity dynamics in $\mathcal{I}$ with $\ddot{p}^i = u^i$

$$u^i = gE_3 - \begin{bmatrix} s_\phi s_\psi + c_\phi s_\theta c_\psi \\ -s_\phi c_\psi + c_\phi s_\theta s_\psi \\ c_\theta c_\phi \end{bmatrix} \frac{T}{m}.$$

Solving this equation for T, ϕ, and θ gives

$$T = m\|u^i - gE_3\| \tag{2a}$$

$$\phi = \arcsin \frac{c_\psi u_2^i - s_\psi u_1^i}{T/m} \tag{2b}$$

$$\theta = \arctan \frac{c_\psi u_1^i + s_\psi u_2^i}{u_3^i - g}. \tag{2c}$$

From (2b) and (2c), we cannot set individual bound for ϕ and θ for any bounds on u_j^i, where $j = 1, 2, 3$. This is due to the expressions' dependence on ψ. If we work in $\mathcal{B}$, the velocity dynamics does not have explicit ψ dependence and this allows us to bound ϕ and θ. See (9) and (13a) below. In addition, the work in this brief can be used to solve image-based visual servoing problems when a camera is fixed to the UAV [30]. In this case, the image kinematics involve both translational and rotational variables, which makes the stabilization of the nonlinear dynamics a challenge. However, existing nonlinear approaches use state transformations, such as spherical coordinates [8], [30], or a virtual camera [31], to put the system into the same form as considered in this brief.

III. Controller Design

Initially, the control objective is to asymptotically regulate a desired constant position p_d^i in $\mathcal{I}$ for any initial position. The stabilization is performed accounting for bounds on thrust, roll, and pitch. The desired position in $\mathcal{B}$ is $p_d^b = R^T p_d^i$ and evolves according to $\dot{p}_d^b = -\mathrm{sk}(\omega^b) p_d^b$. Defining $\delta_1 = p^b - p_d^b$, we obtain

$$\dot{\delta}_1 = -\mathrm{sk}(\omega^b)\delta_1 + v^b. \tag{3}$$

To achieve our control objective, we consider the inner–outer loop control structure, as shown in Fig. 2, to stabilize the dynamics (1b)–(1d) and (3). This structure is chosen, since the rotational dynamics (1c) and (1d) is independent of translational variables. The inner loop tracks a reference roll ϕ_d and

pitch θ_d, which are calculated by the outer loop. A reference yaw ψ_d is provided to the inner loop. The outer loop generates a saturated thrust and bounded references ϕ_d and θ_d, which globally stabilize the translational dynamics.

A. Outer Loop Control

One of the advantages of using translational dynamics in $\mathcal{B}$ is that ψ does not appear explicitly. On the other hand, as shown in (1b) and (3), the inner loop variable ω^b appears. Thus, many saturation methods developed, e.g., [32] and [33], cannot be applied directly. Fortunately, the term involving ω^b depends on $\mathrm{sk}(\omega^b)$, which is skew-symmetric. Thus $x^T \mathrm{sk}(\omega^b)x = 0$, $\forall x \in \mathbb{R}^3$. Therefore, it is possible to eliminate ω^b dependence in the derivative of a quadratic Lyapunov function used for the stability analysis. We extend the nested saturation approach for the chain of integrators developed in [24] to our case. The approach can be seen as a vector form of the nested saturation method because all variables are 3-D vectors. In [34] and [35], the nested saturation method has been used for vector variables. The situation is different here because from (1b) or (3), the three components of the vector δ_1 or v^b are coupled due to the term involving $\mathrm{sk}(\omega^b)$. Thus, they cannot be separately treated as three decoupled second-order systems as in [34]. Azinheira and Moutinho [35] consider a fully actuated airship UAV, which uses a norm to transform the state vector into a scalar. However, the method leads to a nonsmooth input, which complicates tracking in the inner loop if the derivatives of the reference angle are required.

We start with the state and input transformations $y_1 = [y_{1,1},\ y_{1,2},\ y_{1,3}]^T = k_2\delta_1 + v^b$, $y_2 = [y_{2,1},\ y_{2,2},\ y_{2,3}]^T = v^b$, and $u = gR^T E_3 - (T/m)e_3$, where $k_2 > 0$ is a control gain. Hence, (1b) and (3) become

$$\dot{y}_1 = -\mathrm{sk}(\omega^b)y_1 + k_2 y_2 + u \tag{4a}$$

$$\dot{y}_2 = -\mathrm{sk}(\omega^b)y_2 + u. \tag{4b}$$

Based on the nested saturation method [24], we choose the outer loop control

$$u = [u_1, u_2, u_3]^T = -\Sigma_2(k_2 y_2 + \Sigma_1(k_1 y_1)) \tag{5}$$

where $k_1 > 0$ is a control gain, $\Sigma_i([s_1, s_2, s_3]^T) = [\sigma_{i,1}(s_1), \sigma_{i,2}(s_2), \sigma_{i,3}(s_3)]^T$, and $\sigma_{i,j}$ is a saturation function with the following properties:

1) $\sigma_{i,j}$ is continuous and nondecreasing;
2) $s\sigma_{i,j}(s_j) > 0$ for all $s_j \neq 0$;
3) $\sigma_{i,j}(s_j) = s_j$ for all $|s_j| \leq L_{i,j}$;
4) $|\sigma_{i,j}(s_j)| \leq M_{i,j}$ for all $s_j \in \mathbb{R}$;
5) $M_{1,j} = bL_{2,j}$, where $0 < b < 1$.

The following theorem states the stability result for the outer loop.

Theorem 1: There exist b, k_1, k_2, and $L_{2,j}$, $1 \leq j \leq 3$, such that the outer loop dynamics (4) is globally asymptotically stable with the bounded control (5).

Proof: The derivative of the Lyapunov function $V_2 = (1/2)y_2^T y_2$ is $\dot{V}_2 = -y_2^T \Sigma_2(k_2 y_2 + \Sigma_1(k_1 y_1)) = -\sum_{j=1}^{3} y_{2,j}\sigma_{2,j}(k_2 y_{2,j} + \sigma_{1,j}(k_1 y_{1,j}))$. Define a set $Q_2 = \{y_2 \in \mathbb{R}^3 : k_2|y_{2,j}| \leq M_{1,j} + aL_{2,j},\ j = 1, 2, 3\}$, where $a > 0$ is to be determined. Now, we prove that $\dot{V}_2 < 0$ for all $y_2 \notin Q_2$. Since $k_2 y_2$ has three components, we break the proof into three cases.

Case 1: The magnitudes of all three elements of $k_2 y_2$ are larger than $M_{1,j} + aL_{2,j}$, i.e., $|k_2 y_{2,j}| > M_{1,j} + aL_{2,j}$, where $j = 1, 2, 3$. Then, $|k_2 y_{2,j} + \sigma_{1,j}(k_1 y_{1,j})| \geq |k_2 y_{2,j}| - |\sigma_{1,j}(k_1 y_{1,j})| > M_{1,j} + aL_{2,j} - M_{1,j} = aL_{2,j}$ and the sign of $k_2 y_{2,j} + \sigma_{1,j}(k_1 y_{1,j})$ is always determined by $y_{2,j}$, thus $-y_{2,j}\sigma_{2,j}(k_2 y_{2,j} + \sigma_{1,j}(k_1 y_{1,j}))$ is always negative. Therefore

$$\dot{V}_2 < -aL_{2,1}|y_{2,1}| - aL_{2,2}|y_{2,2}| - aL_{2,3}|y_{2,3}| < 0.$$

Case 2: The magnitude of one element of $k_2 y_2$ is less than or equal to $M_{1,j} + aL_{2,j}$. Here, the element $k_2 y_{2,1}$ is considered, i.e., $|k_2 y_{2,1}| \leq M_{1,1} + aL_{2,1}$ and $|k_2 y_{2,j}| > M_{1,j} + aL_{2,j}$, for $j = 2, 3$. Then

$$\begin{aligned} |k_2 y_{2,1} + \sigma_{1,1}(k_1 y_{1,1})| &\leq |k_2 y_{2,1}| + |\sigma_{1,1}(k_1 y_{1,1})| \\ &= 2M_{1,1} + aL_{2,1} \\ &= (2b + a)L_{2,1} \leq L_{2,1} \end{aligned}$$

if

$$2b + a \leq 1 \tag{6}$$

then $\sigma_{2,1}$ is evaluated in its linear region, thus

$$\begin{aligned} \dot{V}_2 &= -y_{2,1}(k_2 y_{2,1} + \sigma_{1,1}(k_1 y_{1,1})) \\ &\quad - \sum_{j=2}^{3} y_{2,j}\sigma_{2,j}(k_2 y_{2,j} + \sigma_{1,j}(k_1 y_{1,j})) \\ &< -k_2 y_{2,1}^2 + M_{1,1}|y_{2,1}| - aL_{2,2}|y_{2,2}| - aL_{2,3}|y_{2,3}| \\ &< -k_2 y_{2,1}^2 + \frac{1}{k_2}M_{1,1}(M_{1,1} + aL_{2,1}) \\ &\quad - \frac{1}{k_2}aL_{2,2}(M_{1,2} + aL_{2,2}) - aL_{2,3}|y_{2,3}| \\ &= -k_2 y_{2,1}^2 + \frac{1}{k_2}\left[\left(1 + \frac{a}{b}\right)M_{1,1}^2 - a(a+b)L_{2,2}^2\right] \\ &\quad - aL_{2,3}|y_{2,3}| < 0 \end{aligned}$$

if $(1 + (a/b))M_{1,1}^2 - a(a+b)L_{2,2}^2 < 0$, i.e., $M_{1,1} < \sqrt{ab}L_{2,2}$. Since $y_{2,1}$ was chosen arbitrarily above, the general condition is $\max_j M_{1,j} < \sqrt{ab}\min_j L_{2,j}$.

Case 3: The magnitudes of two elements of $k_2 y_2$ are no greater than $M_{1,j} + aL_{2,j}$. Suppose they are the first two elements, i.e., $|k_2 y_{2,j}| \leq M_{1,j} + aL_{2,j}$, for $j = 1, 2$ and $|k_2 y_{2,3}| > M_{1,3} + aL_{2,3}$. Similarly

$$\begin{aligned} \dot{V}_2 &= -\sum_{j=1}^{2} y_{2,j}(k_2 y_{2,j} + \sigma_{1,j}(k_1 y_{1,j})) \\ &\quad - y_{2,3}\sigma_{2,3}(k_2 y_{2,3} + \sigma_{1,3}(k_1 y_{1,3})) \\ &< -k_2 y_{2,1}^2 + M_{1,1}|y_{2,1}| - k_2 y_{2,2}^2 + M_{1,2}|y_{2,2}| \\ &\quad - aL_{2,3}|y_{2,3}| \\ &< -k_2 y_{2,1}^2 + \frac{1}{k_2}M_{1,1}(M_{1,1} + aL_{2,1}) - k_2 y_{2,2}^2 \\ &\quad + \frac{1}{k_2}M_{1,2}(M_{1,2} + aL_{2,2}) - \frac{1}{k_2}aL_{2,3}(M_{1,3} + aL_{2,3}) \\ &= -k_2 y_{2,1}^2 - k_2 y_{2,2}^2 \\ &\quad + \frac{1}{k_2}\left[\left(1 + \frac{a}{b}\right)\left(M_{1,1}^2 + M_{1,2}^2\right) - a(a+b)L_{2,3}^2\right] < 0 \end{aligned}$$

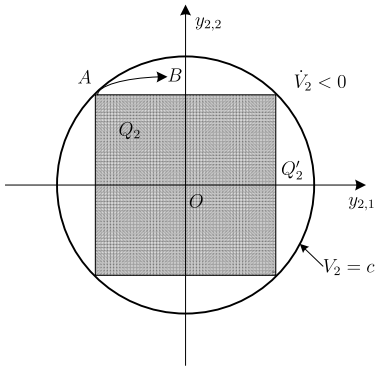

Fig. 3. Relation between Q_2 and Q_2'.

if

$$\max_j M_{1,j} < \sqrt{\frac{ab}{2}} \min_j L_{2,j}. \tag{7}$$

We remark Q_2 is not an invariant set. As shown in Fig. 3, where for simplification only the $y_{2,1}$ and $y_{2,2}$ components are shown, the trajectory of y_2 may go from point A to B because $V_2(A) > V_2(B)$. Evidently, $B \notin Q_2$. The smallest invariant set that contains Q_2 is defined as $Q_2' = \{y_2' : V_2(y_2') \le c, c = \max_{y_2 \in Q_2} V_2(y_2)\}$. Therefore, based on the analysis above, we conclude that y_2 will enter Q_2' in finite time and remains there. Now, we need to ensure Q_2' is enclosed in the region where $\sigma_{2,j}$ is linear.

Within Q_2', the maximum norm of y_2 is $(\Sigma_{j=1}^3((M_{1,j} + aL_{2,j})/k_2)^2)^{1/2} = ((a+b)/k_2)(\Sigma_{j=1}^3 L_{2,j}^2)^{1/2}$. If

$$(a+b)\sqrt{\Sigma_{j=1}^3 L_{2,j}^2} \le \min_j L_{2,j} - b \max_j L_{2,j} \tag{8}$$

then $|k_2 y_{2,j} + \sigma_{1,j}(k_1 y_{1,j})| \le (a+b)(\Sigma_{j=1}^3 L_{2,j}^2)^{1/2} + M_{1,j} \le \min_j L_{2,j} - b \max_j L_{2,j} + \max_j M_{1,j} \le L_{2,j}$. Therefore, $\sigma_{2,j} = k_2 y_{2,j} + \sigma_{1,j}(k_1 y_{1,j})$, where $j = 1, 2, 3$ within Q_2'.

For (4a), we consider the Lyapunov function $V_1 = (1/2) y_1^T y_1$ so that $\dot{V}_1 = y_1^T(k_2 y_2 + \Sigma_2(k_2 y_2 + \Sigma_1(k_1 y_1)))$. From the discussion above, we know y_2 will eventually converge to the invariant set Q_2' and the trajectory of y_2 is bounded. Thus, in the region where $\|y_1\| \ge \|k_2 y_2 + \Sigma_2(k_2 y_2 + \Sigma_1(k_1 y_1))\|$, we have $\dot{V}_1 \le \|y_1\| \|k_2 y_2 + \Sigma_2(k_2 y_2 + \Sigma_1(k_1 y_1))\| \le \|y_1\|^2 = 2V_1$. From Gronwall–Bellman inequality, $V_1(t) \le V_1(t_0) e^{2(t-t_0)}$, where t_0 is the time when $\|y_1\| \ge \|y_2 + \Sigma_2(k_2 y_2 + \Sigma_1(k_1 y_1))\|$ for $t > t_0$. Therefore, in finite time, V_1 is bounded, which implies the boundedness of y_1.

After y_2 enters Q_2', (5) becomes $u = -k_2 y_2 - \Sigma_1(k_1 y_1)$. Thus, $\dot{y}_1 = -\mathrm{sk}(\omega^b) y_1 - \Sigma_1(k_1 y_1)$. The derivative of the Lyapunov function V_1 along the trajectory of y_1 is always negative because $\dot{V}_1 = -y_{1,1}\sigma_{1,1}(k_1 y_{1,1}) - y_{1,2}\sigma_{1,2}(k_1 y_{1,2}) - y_{1,3}\sigma_{1,3}(k_1 y_{1,3}) \le 0$, and $\dot{V}_1 < 0$, for all $y_1 \ne 0$. Thus, $y_{1,j}$ will enter the linear region of $\sigma_{1,j}$.

When $\sigma_{1,j}$ and $\sigma_{2,j}$ are linear, then (4) becomes $\dot{y}_1 = -\mathrm{sk}(\omega^b) y_1 - k_1 y_1$ and $\dot{y}_2 = -\mathrm{sk}(\omega^b) y_2 - k_1 y_1 - k_2 y_2$. For the Lyapunov function $V_3 = V_1 + V_2$, we have $\dot{V}_3 = -k_1 y_1^T y_1 - k_1 y_1^T y_2 - k_2 y_2^T y_2 = -k_1(y_1 + (1/2) y_2)^T (y_1 + (1/2) y_2) - (k_2 - (1/4) k_1) y_2^T y_2 < 0$ if the gains satisfy $k_2 > k_1/4$, then the equilibrium of (4) and (5) is globally asymptotically stable.

If $L_{2,1} = L_{2,2} = L_{2,3}$, the values of a and b can be given explicitly. Conditions (6)–(8) can be simplified to $2b + a \le 1$, $2b < a$, and $(\sqrt{3} + 1)b + \sqrt{3}a \le 1$. This yields $b < (1/(1 + 3\sqrt{3}))$ and $2b < a \le (1/\sqrt{3}) - (1 + (1/\sqrt{3}))b$. We can guarantee the existence of $M_{i,j}$ and $L_{i,j}$, since for all $M_{2,j}$, we can always choose $L_{2,1} = L_{2,2} = L_{2,3} = \min_j M_{2,j} - \varepsilon$, where ε is taken sufficiently small. ■

Based on the outer loop controller, the reference angles to the inner loop and thrust T can be calculated as

$$\theta_d = -\arcsin \frac{u_1}{g} \tag{9a}$$

$$\phi_d = \arcsin \frac{u_2}{g c_{\theta_d}} \tag{9b}$$

$$T = m(g c_{\theta_d} c_{\phi_d} - u_3). \tag{9c}$$

Remark 1: In the design process, we typically begin with bounds on roll ϕ_m, pitch θ_m, and thrust T_m. Next, we calculate the bound $u_m = [u_{m,1}, u_{m,2}, u_{m,3}]^T$ of u according to $u_{m,1} = g s_{\theta_m}$, $u_{m,2} = g c_{\theta_m} s_{\phi_m}$, and $u_{m,3} = (T_m/m) - g$, then we choose $L_{2,j}$ and $M_{2,j}$ satisfying $L_{2,j} < M_{2,j} \le u_{m,j}$ and b based on conditions (6)–(8).

Remark 2: To remove the steady-state error, which arises in practice (e.g., due to attitude estimate error), the control can be augmented with an integrator state ξ satisfying $\dot{\xi} = -\mathrm{sk}(\omega^b)\xi + \delta_1$. By redefining $y_1 = k_2 k_3 \xi + (k_2 + k_3)\delta_1 + v^b$, $y_2 = k_3 \delta_1 + v^b$, and $y_3 = v^b$, we obtain the augmented error system

$$\begin{aligned} \dot{y}_1 &= -\mathrm{sk}(\omega^b) y_1 + k_2 y_2 + k_3 y_3 + u \\ \dot{y}_2 &= -\mathrm{sk}(\omega^b) y_2 + k_3 y_3 + u \\ \dot{y}_3 &= -\mathrm{sk}(\omega^b) y_3 + u. \end{aligned}$$

Then, the controller

$$u = -\Sigma_3(k_3 y_3 + \Sigma_2(k_2 y_2 + \Sigma_1(k_1 y_1))) \tag{10}$$

will globally asymptotically stabilize the outer loop provided

$$\begin{bmatrix} k_1 & \frac{k_1}{2} & \frac{k_1}{2} \\ \frac{k_1}{2} & k_2 & \frac{k_2}{2} \\ \frac{k_1}{2} & \frac{k_2}{2} & k_3 \end{bmatrix} > 0. \tag{11}$$

This condition is satisfied with $k_1 > 0$, $k_2 > k_1/4$, and $k_3 > k_2^2/(4k_2 - k_1)$.

Remark 3: For simplicity, we use scalar gains k_i in (10). However, it is possible to generalize to matrix gains $K_i = \mathrm{diag}(k_{i,1}, k_{i,2}, k_{i,3})$, where $i = 1, 2, 3$. In this case, we have three conditions on the gain matrices, which are similar to (11) with k_i replaced by $k_{i,j}$, where $j = 1, 2, 3$.

The proposed control can be extended to the constrained output tracking problems, where p_d^i is a time-varying function in $\mathcal{I}$.

Corollary 1: Suppose the desired position $p_d^i(t) = [p_{d,1}^i(t), p_{d,2}^i(t), p_{d,3}^i(t)]^T$ is such that $\ddot{p}_{d,1}^i = \ddot{p}_{d,2}^i = 0$ and $|\ddot{p}_{d,3}^i| \le \epsilon < g$. Then, there exists a bounded control, which asymptotically tracks p_d^i and satisfies constraints $|\phi_d| \le \phi_m$, $|\theta_d| \le \theta_m$, and $|T| \le T_m$, where $\phi_m, \theta_m < 90°$, $T_m > m(g + \epsilon)$.

Proof: The trajectory of p_d^i in $\mathcal{B}$ is $p_d^b = R^T p_d^i$ and $\dot{p}_d^b = R^T \dot{p}_d^i + \dot{R}^T p_d^i = -\mathrm{sk}(\omega^b) p_d^b + R^T \dot{p}_d^i$. By defining $\tilde{\delta}_1 = p^b - p_d^b$ and $\tilde{\delta}_2 = v^b - R^T \dot{p}_d^i$, we obtain

$$\dot{\tilde{\delta}}_1 = -\mathrm{sk}(\omega^b)\tilde{\delta}_1 + \tilde{\delta}_2 \tag{12a}$$

$$\dot{\tilde{\delta}}_2 = -\mathrm{sk}(\omega^b)\tilde{\delta}_2 + \tilde{u} \tag{12b}$$

where $\tilde{u} = (g - \ddot{p}_{d,3}^i)R^T E_3 - (T/m)e_3$. From Theorem 1, there exists a bounded controller $\tilde{u} = -\tilde{\Sigma}_2(\tilde{k}_2\tilde{\delta}_2 + \tilde{\Sigma}_1(\tilde{k}_1\tilde{k}_2\tilde{\delta}_1 + \tilde{k}_1\tilde{\delta}_2))$ stabilizing dynamics (12). The parameters $\tilde{M}_{2,j}$ of $\tilde{\Sigma}_2$ can be chosen as $\tilde{M}_{2,1} \leq (g-\epsilon)s_{\theta_m}$, $\tilde{M}_{2,2} \leq (g-\epsilon)c_{\theta_m}s_{\phi_m}$, and $\tilde{M}_{2,3} \leq T_m/m - (g+\epsilon)$. The remaining parameters in $\tilde{\Sigma}_1$ and $\tilde{\Sigma}_2$ can be determined following the same procedure in Remark 1. Next, the thrust, and reference roll and pitch are

$$\theta_d = -\arcsin\frac{\tilde{u}_1}{g - \ddot{p}_{d,3}^i} \tag{13a}$$

$$\phi_d = \arcsin\frac{\tilde{u}_2}{(g - \ddot{p}_{d,3}^i)c_{\theta_d}} \tag{13b}$$

$$T = m((g - \ddot{p}_{d,3}^i)c_{\theta_d}c_{\phi_d} - \tilde{u}_3). \tag{13c}$$

The proof of boundedness is straightforward, e.g., $|\theta_d| \leq |\arcsin(\tilde{M}_{2,1}/(g - \ddot{p}_{d,3}^i))| \leq |\arcsin((g-\epsilon)s_{\theta_m})/(g - \ddot{p}_{d,3}^i)| \leq |\arcsin s_{\theta_m}| = \theta_m$. ∎

Remark 4: When $\ddot{p}_{d,1}^i, \ddot{p}_{d,2}^i \neq 0$ and are bounded, $\tilde{u}$ becomes $\tilde{u} = R^T(gE_3 - \ddot{p}_d^i) - (T/m)e_3$, therefore, the reference angles θ_d and ϕ_d cannot be solved using (13a) and (13b). However, we can treat the term $R^T[\ddot{p}_{d,1}^i, \ddot{p}_{d,2}^i, 0]^T$ as a disturbance whose bound is determined by $\ddot{p}_{d,1}^i$ and $\ddot{p}_{d,2}^i$. As long as $\max\{|\ddot{p}_{d,1}^i|, |\ddot{p}_{d,2}^i|\} < \min\{M_{2,1}, M_{2,2}\}$, a bounded tracking result can be guaranteed and the tracking performance is determined by the bounds of $\ddot{p}_{d,1}^i$ and $\ddot{p}_{d,2}^i$.

B. Inner Loop Controller

The control design of the rotational dynamics subsystem is well studied [9], [29]. Our approach uses a simple PID controller to track given angles ϕ_d, θ_d, and ψ_d. The roll and pitch setpoints are from (9a), (9b) or (13a), (13b). The yaw reference is provided externally. We assume $\dot{\psi}_d$ and $\ddot{\psi}_d$ are bounded and known. By defining $e_\eta = \eta - \eta_d$, where $\eta_d = [\phi_d, \theta_d, \psi_d]^T$, the inner loop can be written as

$$\dot{e}_\eta = e_\omega + d_1$$
$$\dot{e}_\omega = \bar{\tau}^b + d_2$$

where $e_\omega = W\omega^b - \bar{E}_3\dot{\eta}_d$, $d_1 = -\bar{E}_{12}\dot{\eta}_d$, $\bar{\tau}^b = \dot{W}\omega + W(-J^{-1}\omega^b \times J\omega^b + J^{-1}\tau^b) - \bar{E}_3\ddot{\eta}_d$, $d_2 = -\bar{E}_{12}\ddot{\eta}_d$, $\bar{E}_{12} = \mathrm{diag}([1,1,0])$, and $\bar{E}_3 = \mathrm{diag}([0,0,1])$. We treat d_1 and d_2 as disturbances. One reason for introducing d_1 and d_2 as disturbances is to avoid the control having dependence on the first and second derivatives of θ_d and ϕ_d. Computing these derivatives would introduce noise to the closed loop, which decreases its performance. The computation of $\dot{\phi}_d, \ddot{\phi}_d, \dot{\theta}_d$, and $\ddot{\theta}_d$ is commonly avoided in practice for that reason [19], [36].

The inner loop PID controller is given by

$$\bar{\tau}^b = -k_p^a e_\eta - k_i^a \int_0^t e_\eta(\tau)d\tau - k_d^a e_\omega \tag{14}$$

where $k_p^a, k_i^a, k_d^a \in \mathbb{R}^{3\times 3}$. Then, we can calculate the actual control torque τ^b using (14)

With Lyapunov function $V_4 = (\alpha/2)\int_0^t e_\eta^T(\tau)d\tau k_i^a \int_0^t e_\eta(\tau)d\tau + e_\eta^T k_i^a \int_0^t e_\eta(\tau)d\tau + (1/2)e_\eta^T(k_p^a + \alpha k_d^a)e_\eta + \alpha e_\eta^T e_\omega + (1/2)e_\omega^T e_\omega$ and $\dot{V}_4 = -e_\eta^T(\alpha k_p^a - k_i^a)e_\eta - e_\omega^T(k_d^a - \alpha I_3)e_\omega$, where I_3 is an identity matrix, the inner loop with $d_1 = d_2 = 0$ can be exponentially stabilized with (14) if $\alpha k_p^a > k_i^a$ and $k_d^a > \alpha I_3$.

Other parameterizations of the rotation matrix R have been used to design the inner loop. For example, rotation matrices [29] or quaternions [9] avoid Euler angle singularities and provide almost global stabilization results. We choose Euler angles, since they lead to a simple PID control structure for the inner loop. This simplicity provides practical benefits, such as ease of tuning, reduced computational complexity for on-board implementation, and robustness to disturbances [11]. Euler angles have been widely used in [26]–[28] and [37] and are standard on most field tested autopilots [2], [13]. The ZYX Euler angles have singularities at $\theta = (\pi/2) + n\pi, n \in \mathbb{Z}$, which can be avoided using the saturated control proposed in this brief.

C. Closed-Loop Stability Analysis

In this section, we analyze the effect of the inner loop tracking error on closed-loop stability. The closed-loop system is given by

$$\dot{y}_1 = -\mathrm{sk}(\omega^b)y_1 + k_2 y_2 + u + \delta_\eta \tag{15a}$$

$$\dot{y}_2 = -\mathrm{sk}(\omega^b)y_2 + u + \delta_\eta \tag{15b}$$

$$\dot{e}_\eta = e_\omega + d_1 \tag{15c}$$

$$\dot{e}_\omega = \bar{\tau}^b + d_2 \tag{15d}$$

where u and $\bar{\tau}^b$ are given in (5) and (14), respectively, and $\delta_\eta = g[s_{\theta_d} - s_\theta, c_\theta s_\phi - c_{\theta_d}s_{\phi_d}, c_\theta c_\phi - c_{\theta_d}c_{\phi_d}]^T$. Hence, $\|\delta_\eta\| < c_1\|\bar{E}_{12}e_\eta\|$. We consider a region where $\|e_\eta\| < \zeta_\eta$ and $\|e_\omega\| < \zeta_\omega$, and use the linear approximation of d_1 and d_2, i.e., $d_1 \approx (1/g)\dot{u}\bar{E}_{21}$ and $d_2 \approx (1/g)\ddot{u}\bar{E}_{21}$, where

$$\bar{E}_{21} = \begin{bmatrix} 0 & 1 & 0 \\ 1 & 0 & 0 \\ 0 & 0 & 0 \end{bmatrix}.$$

Moreover, we assume $\dot{\sigma}_{i,j}(x), \ddot{\sigma}_{i,j}(x) = 0$, for $|x| > \zeta_{i,j} + L_{i,j}$.

First, we consider the case when the control is saturated with $\dot{\Sigma}_2, \ddot{\Sigma}_2 = 0$, i.e., $|y_{2,j}| > \zeta_{2,j} + L_{2,j} + M_{1,j}$. Hence, $d_1, d_2 = 0$. From Section III-B, we know that the inner loop is exponentially stable, thus there exists a time T^*, such that $\|\delta_\eta(t)\| < c_1\|\bar{E}_{12}e_\eta(t)\| < \min_j \zeta_{2,j}$, for all $t > T^*$. With the Lyapunov function V_2, we have

$$\dot{V}_2 < -\sum_{j=1}^{3} |y_{2,j}|(\zeta_{2,j} + L_{2,j} - \|\delta_\eta\|) < 0.$$

Next, we consider the case when some components of Σ_2 become linear, e.g., $\sigma_{2,1}$ and $\sigma_{2,2}$. Then, $d_1 = (1/g)(k_2^2 y_2 + f_1(e_\omega)y_2)\bar{E}_{21}$ and $d_2 = (1/g)(-k_2^3 y_2 + f_2(e_\eta, e_\omega)y_2)\bar{E}_{21}$. Since $\|e_\eta\| < \zeta_\eta$ and $\|e_\omega\| < \zeta_\omega$, we have $\|f_1\| < \bar{f}_1$

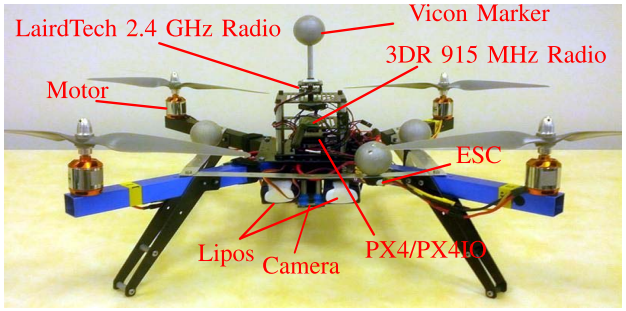

Fig. 4. The ANCL quadrotor UAV.

and $\|f_2\| < \bar{f}_2$. Thus, based on the Lyapunov function $V_5 = V_2 + V_4$, we have

$$\begin{aligned}\dot{V}_5 < & -k_2 y_{2,1}^2 - k_2 y_{2,2}^2 + \sum_{j=1}^{2} |y_{2,j}|(M_{1,j} + \|\delta_\eta\|) \\ & -|y_{2,3}|(L_{2,3} + \zeta_{2,3} - \|\delta_\eta\|) - e_\eta^T \left(\alpha k_p^a - k_i^a\right) e_\eta \\ & -e_\omega^T \left(k_d^a - \alpha I_3\right) e_\omega + \frac{1}{g} \sum_{j=1}^{2} \left(k_2^2 + \bar{f}_1\right) |y_{2,j}| \|e_\eta\| \\ & + \frac{1}{g} \sum_{j=1}^{2} \left(-k_2^3 + \bar{f}_2\right) |y_{2,j}| \|e_\omega\|.\end{aligned}$$

If $2(\max_j M_{1,j} + c_1\zeta_\eta) < \min_j L_{2,j}$ and $\min_j \zeta_{2,j} > c_1\zeta_\eta$, then we can find α, k_p^a, k_i^a, k_d^a, ζ_η, and ζ_ω, such that $\dot{V}_5 < 0$. Similarly, we can use the same method of proof for the other cases. Then, we can conclude that the saturation function Σ_2 will become linear. The same procedure can be used to prove that Σ_1 will become linear eventually.

After Σ_1 and Σ_2 become linear, (15a) and (15b) become

$$\begin{aligned}\dot{y}_1 &= -\text{sk}(\omega^b) y_1 - k_1 y_1 + \delta_\eta \\ \dot{y}_2 &= -\text{sk}(\omega^b) y_2 - k_1 y_1 - k_2 y_2 + \delta_\eta.\end{aligned}$$

In this case, d_1 and d_2 can be written as $d_1 = (1/g)(k_2^2 y_2 + (k_1 k_2 + k_1^2) y_1 + g_1(e_\omega) y_1 + g_2(e_\omega) y_2)) \bar{E}_{21}$ and $d_2 = (1/g)(-k_2^3 y_2 - (k_1 k_2^2 + k_1^2 k_2 + k_1^3) y_1 + h_1(e_\eta, e_\omega) y_1 + h_2(e_\eta, e_\omega) y_2)) \bar{E}_{21}$, where g_1, g_2, h_1, and h_2 are bounded. The asymptotic stability can be proved using the Lyapunov function $V_6 = V_3 + V_4$, since $\dot{V}_6 \leq -k_1 y_1^T y_1 - k_1 y_1^T y_2 - k_2 y_2^T y_2 + c_1 \|e_\eta\| \|y_1\| + c_1 \|e_\eta\| \|y_2\| - e_\eta^T (\alpha k_p^a - k_i^a) e_\eta - e_\omega^T (k_d^a - \alpha I_3) e_\omega + e_\eta^T d_1 + e_\omega^T d_2$. The last two terms are the dot products of y_1, y_2 and e_η, e_ω. Therefore, there always exists α, k_p^a, k_i^a, k_d^a, ζ_η, and ζ_ω, such that $\dot{V}_6 < 0$. We can conclude that the closed-loop system is locally asymptotic stable, i.e., for any $y_1, y_2 \in \mathbb{R}^3$, and $e_\eta(0)$ and $e_\omega(0)$ sufficiently close to 0, the state of the closed loop (15) converges to 0.

IV. Experiments

In this section the proposed controller is tested on the indoor ANCL quadrotor platform at the University of Alberta. The platform consists of an indoor quadrotor vehicle, as shown in Fig. 4, a Vicon motion capture system to estimate pose and linear velocity of the vehicle, and a PC ground station running QGroundControl [38]. Details of the test stand can be found in [12]. The on-board autopilot is based on the PX4FMU, which includes a 168-MHz ARM processor, a 3-D accelerometer, a 3-D gyroscope, a 3-D magnometer, and a pressure sensor. The PX4IO is connected to the PX4FMU and provides various hardware interfaces and a power supply. The quadrotor uses Afro 30-A electronic speed controllers, Turnigy 1100-kV brushless outrunner motors, and APC 12-in multirotor propellers. A 3DRobotics 915-MHz radio provides communication to the ground station, and a LairdTech 2.4-GHz radio communicates with the Vicon system. Manual control of the vehicle is possible with a Sperktrum radio and receiver. The quadrotor weighs 1.6 kg and is powered by two 2600-mAh LiPo batteries.

TABLE I
Controller Parameters

k_1	1.0
k_2	0.8
k_3	3.6
$M_{3,j}$	4.5
b	0.1614
$L_{i,j}$	$0.95 M_{i,j}$

We consider two different cases: hovering and tracking linear reference outputs. For both cases we use the same inner loop control law. Note that the inner loop gains correspond to a normalized control signal as in [39]. We remark that in our experiment, we neglect the nonlinear terms in τ^b, i.e., we use $\tau^b \approx J\bar{\tau}^b$. The saturation function $\sigma_{i,j}$ chosen in the outer loop is

$$\sigma_{i,j}(x) = \begin{cases} x, & \text{if } |x| \leq L_{i,j} \\ \text{sign}(x)\left(L_{i,j} + \dfrac{\beta_{i,j} - \beta_{i,j} e^{-2(|x| - L_{i,j})}}{1 + (2\beta_{i,j} - 1) e^{-2(|x| - L_{i,j})}}\right), & \text{otherwise} \end{cases}$$

where $\text{sign}(x)$ is the sign function and $\beta_{i,j} = M_{i,j} - L_{i,j}$.

A. Case 1: Hovering

The desired position is set to $p_d^i = [0, 0, -1.2]^T$ m. The desired yaw is $\psi_d = 0°$. Initially the quadrotor is manually controlled to fly near the origin of $\mathcal{I}$. The nested saturation controller is switched ON at around $t = 31$ s and switched OFF at around $t = 59$ s. To remove steady state error, the augmented controller with integral term (10) is used. We set the bound for pitch $\theta_m = 27.3°$. This leads to $M_{3,1} = g s_{\theta_m} \approx 4.5$. For simplicity, we choose $M_{3,1} = M_{3,2} = M_{3,3}$, which means we obtain bounds $\phi_m = \arcsin(t_{\theta_m}) \approx 31.1°$ and $T_m = m(g + M_{3,1}) \approx 22.9$ N. Parameters for the controller are listed in Table I. Fig. 5 gives the position trajectories of the quadrotor and thrust input. The average magnitudes of the steady-state error in p_1^i and p_2^i are 1.5 and 3.5 cm, respectively. The trajectories of ϕ, θ, and ψ are shown in Fig. 6. In the figures we use dashed-dotted blue lines to denote the desired value and solid red lines for the actual value.

B. Case 2: Tracking Linear Trajectories

The reference trajectory is chosen as a triangle, which satisfies the conditions in Corollary 1 on each edge.

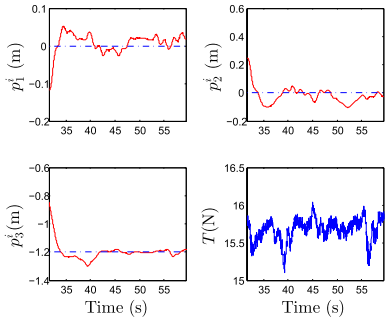

Fig. 5. Case 1: trajectories of position p^i and thrust T.

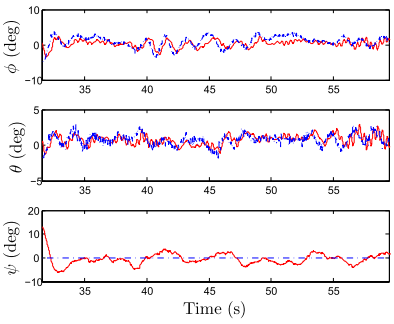

Fig. 6. Case 1: trajectories of ϕ, θ, and ψ.

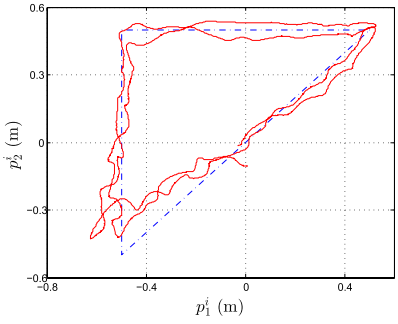

Fig. 7. Case 2: position trajectory in the $p_1^i - p_2^i$ plane.

The vertices of the triangle are set to $[0.5, 0.5, -1.2]^T$ m, $[-0.5, 0.5, -1.2]^T$ m, and $[-0.5, -0.5, -1.2]^T$ m. The desired velocity is 0.08 m/s. The quadrotor is manually controlled to hover around $[0, 0, -1.2]^T$ m and switched to the proposed tracking controller at $t = 19$ s. After traveling the triangular path twice, the controller is switched OFF at $t = 104$ s. We use the same controller parameters as in Case 1. The position trajectory of the vehicle in a horizontal plane is given in Fig. 7. To show the tracking performance more precisely, the trajectories of p_1^i and p_2^i versus time are given in Fig. 8. The trajectory of p_3^i is shown in Fig. 9, and Fig. 10 gives the Euler angles and the inner loop references.

We observe that the trajectories for ϕ, θ, and T remain in a range much smaller than the provided bounds ϕ_m, θ_m, and T_m. This is due to the particular initial conditions used, which result in the saturation functions operating in their linear region. Due to the limited space in our lab it is difficult to operate outside the linear region. Therefore, we provide simulation results which illustrate this case. To add more realism to the simulation, we add unmodeled dynamics, including

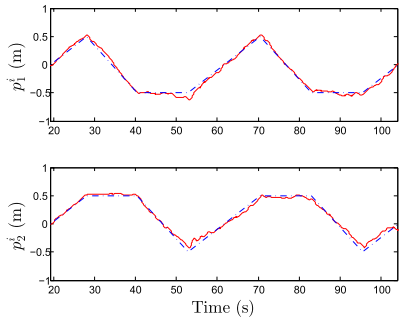

Fig. 8. Case 2: position trajectories p_1^i and p_2^i.

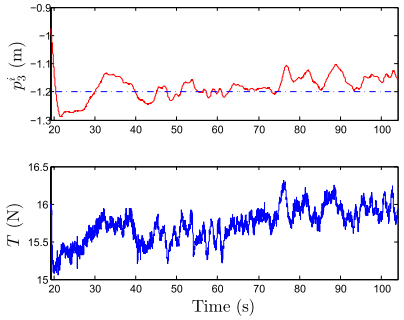

Fig. 9. Case 2: trajectories of the height p_3^i and thrust T.

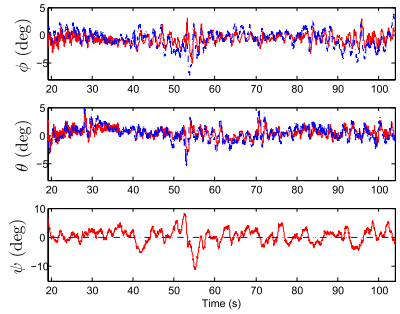

Fig. 10. Case 2: trajectories of ϕ, θ, and ψ.

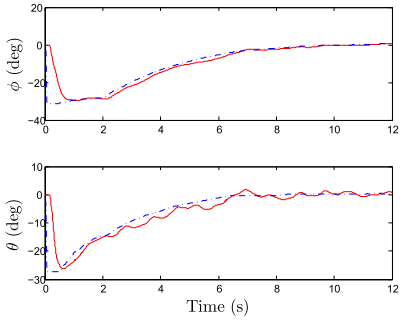

Fig. 11. Trajectories of ϕ and θ for initial velocity $\dot{p}^i(0) = [-9, 9, 0]$ m/s for position regulation.

blade flapping [11], [40], induced drag [41], gyroscopic terms, measurement errors, time delay, and wind turbulence [42]. From Fig. 11, we observe that the reference angles approach their bounds and the stability is achieved.

V. Conclusion

This brief developed a novel inner–outer loop controller with saturated thrust input, roll, and pitch.

The outer loop consists of a nested saturation controller, which is proved to be globally asymptotically stable assuming no inner loop tracking error. The inner loop is based on a commonly used PID control. An analysis of the closed-loop stability accounting for inner loop tracking error is provided. The proposed inner–outer loop controller is implemented on the indoor ANCL quadrotor platform. The robustness of the proposed method is validated for hovering and tracking control objectives.

ACKNOWLEDGMENT

The authors would like to thank G. Fink who provided support for the experimental implementation in this brief.

REFERENCES

[1] F. Kendoul, "Survey of advances in guidance, navigation, and control of unmanned rotorcraft systems," *J. Field Robot.*, vol. 29, no. 2, pp. 315–378, Mar. 2012.

[2] H. Lim, J. Park, D. Lee, and H. J. Kim, "Build your own quadrotor: Open-source projects on unmanned aerial vehicles," *IEEE Robot. Autom. Mag.*, vol. 19, no. 3, pp. 33–45, Sep. 2012.

[3] M.-D. Hua, T. Hamel, P. Morin, and C. Samson, "Introduction to feedback control of underactuated VTOL vehicles: A review of basic control design ideas and principles," *IEEE Control Syst.*, vol. 33, no. 1, pp. 61–75, Feb. 2013.

[4] T. J. Koo and S. Sastry, "Output tracking control design of a helicopter model based on approximate linearization," in *Proc. 37th IEEE Conf. Decision Control*, Tampa, FL, USA, Dec. 1998, pp. 3635–3640.

[5] A. Isidori, L. Marconi, and A. Serrani, "Robust nonlinear motion control of a helicopter," *IEEE Trans. Autom. Control*, vol. 48, no. 3, pp. 413–426, Mar. 2003.

[6] R. Mahony and T. Hamel, "Robust trajectory tracking for a scale model autonomous helicopter," *Int. J. Robust Nonlinear Control*, vol. 14, no. 12, pp. 1035–1059, Aug. 2004.

[7] P. Castillo, R. Lozano, and A. E. Dzul, *Modelling and Control of Mini-Flying Machines*. London, U.K.: Springer-Verlag, 2005.

[8] T. Hamel and R. Mahony, "Visual servoing of an under-actuated dynamic rigid-body system: An image-based approach," *IEEE Trans. Robot. Autom.*, vol. 18, no. 2, pp. 187–198, Apr. 2002.

[9] A. Tayebi and S. McGilvray, "Attitude stabilization of a VTOL quadrotor aircraft," *IEEE Trans. Control Syst. Technol.*, vol. 14, no. 3, pp. 562–571, May 2006.

[10] D. Lee, T. C. Burg, B. Xian, and D. M. Dawson, "Output feedback tracking control of an underactuated quad-rotor UAV," in *Proc. Amer. Control Conf.*, New York, NY, USA, Jul. 2007, pp. 1775–1780.

[11] P. Pounds, R. Mahony, and P. Corke, "Modelling and control of a large quadrotor robot," *Control Eng. Pract.*, vol. 18, no. 7, pp. 691–699, Jul. 2010.

[12] G. Fink, H. Xie, A. F. Lynch, and M. Jagersand, "Nonlinear dynamic image-based visual servoing of a quadrotor," *J. Unmanned Vehicle Syst.*, vol. 3, no. 1, pp. 1–21, Jan. 2015.

[13] Institute for Visual Computing, Swiss Federal Institute of Technology in Zürich. (2015). *PX4 Autopilot*. [Online]. Available: http://pixhawk.org/, accessed Mar. 25, 2015.

[14] N. Mohan, T. M. Undeland, and W. P. Robbins, *Power Electronics: Converters, Applications, and Design*, 3rd ed. New York, NY, USA: Wiley, 2003.

[15] F. Kendoul, I. Fantoni, and R. Lozano, "Asymptotic stability of hierarchical inner-outer loop-based flight controllers," in *Proc. 17th IFAC World Congr.*, Seoul, Korea, Jul. 2008, pp. 1741–1746.

[16] A. Roberts and A. Tayebi, "Adaptive position tracking of VTOL UAVs," *IEEE Trans. Robot.*, vol. 27, no. 1, pp. 129–142, Feb. 2011.

[17] L. Wang and H. Jia, "The trajectory tracking problem of quadrotor UAV: Global stability analysis and control design based on the cascade theory," *Asian J. Control*, vol. 16, no. 2, pp. 574–588, Mar. 2014.

[18] A. Roza and M. Maggiore, "A class of position controllers for underactuated VTOL vehicles," *IEEE Trans. Autom. Control*, vol. 59, no. 9, pp. 2580–2585, Sep. 2014.

[19] B. Godbolt, N. I. Vitzilaios, and A. F. Lynch, "Experimental validation of a helicopter autopilot design using model-based PID control," *J. Intell. Robot. Syst.*, vol. 70, nos. 1–4, pp. 385–399, Apr. 2013.

[20] B. Godbolt and A. F. Lynch, "Model-based helicopter UAV control: Experimental results," *J. Intell. Robot. Syst.*, vol. 73, nos. 1–4, pp. 19–31, Jan. 2014.

[21] F. Mazenc, R. E. Mahony, and R. Lozano, "Forwarding control of scale model autonomous helicopter: A Lyapunov control design," in *Proc. 42nd IEEE Conf. Decision Control*. Maui, HI, USA, Dec. 2003, pp. 3960–3965.

[22] M. Burger and M. Guay, "A backstepping approach to multivariable robust constraint satisfaction with application to a VTOL helicopter," in *Proc. 48th IEEE Conf. Decision Control, 28th Chin. Control Conf.*, Shanghai, China, Dec. 2009, pp. 5239–5244.

[23] P. Castillo, A. Dzul, and R. Lozano, "Real-time stabilization and tracking of a four-rotor mini rotorcraft," *IEEE Trans. Control Syst. Technol.*, vol. 12, no. 4, pp. 510–516, Jul. 2004.

[24] A. R. Teel, "Global stabilization and restricted tracking for multiple integrators with bounded controls," *Syst. Control Lett.*, vol. 18, no. 3, pp. 165–171, Mar. 1992.

[25] N. Metni and T. Hamel, "A UAV for bridge inspection: Visual servoing control law with orientation limits," *Autom. Construction*, vol. 17, no. 1, pp. 3–10, Nov. 2007.

[26] C. Nicol, C. J. B. Macnab, and A. Ramirez-Serrano, "Robust adaptive control of a quadrotor helicopter," *Mechatronics*, vol. 21, no. 6, pp. 927–938, Sep. 2011.

[27] L. Meier, P. Tanskanen, L. Heng, G. H. Lee, F. Fraundorfer, and M. Pollefeys, "PIXHAWK: A micro aerial vehicle design for autonomous flight using onboard computer vision," *Auto. Robots*, vol. 33, nos. 1–2, pp. 21–39, Aug. 2012.

[28] D. Mellinger, N. Michael, and V. Kumar, "Trajectory generation and control for precise aggressive maneuvers with quadrotors," in *Experimental Robotics* (Springer Tracts in Advanced Robotics), vol. 79, O. Khatib, V. Kumar, and G. Sukhatme, Eds. Berlin, Germany: Springer, 2014, pp. 361–373.

[29] F. Bullo and R. M. Murray, "Tracking for fully actuated mechanical systems: A geometric framework," *Automatica*, vol. 35, no. 1, pp. 17–34, Jan. 1999.

[30] T. Hamel and R. Mahony, "Image based visual servo control for a class of aerial robotic systems," *Automatica*, vol. 43, no. 11, pp. 1975–1983, Nov. 2007.

[31] H. Jabbari, G. Oriolo, and H. Bolandi, "An adaptive scheme for image-based visual servoing of an underactuated UAV," *Int. J. Robot. Autom.*, vol. 29, no. 1, pp. 92–104, Jan. 2014.

[32] H. J. Sussmann and Y. Yang, "On the stabilizability of multiple integrators by means of bounded feedback controls," in *Proc. 30th IEEE Conf. Decision Control*, Brighton, U.K., Dec. 1991, pp. 70–72.

[33] F. Mazenc and A. Iggidr, "Backstepping with bounded feedbacks," *Syst. Control Lett.*, vol. 51, nos. 3–4, pp. 235–245, Mar. 2004.

[34] I. A. Raptis, K. P. Valavanis, and W. A. Moreno, "A novel nonlinear backstepping controller design for helicopters using the rotation matrix," *IEEE Trans. Control Syst. Technol.*, vol. 19, no. 2, pp. 465–473, Mar. 2011.

[35] J. R. Azinheira and A. Moutinho, "Hover control of an UAV with backstepping design including input saturations," *IEEE Trans. Control Syst. Technol.*, vol. 16, no. 3, pp. 517–526, May 2008.

[36] S. Bouabdallah, P. Murrieri, and R. Siegwart, "Design and control of an indoor micro quadrotor," in *Proc. IEEE Int. Conf. Robot. Autom.* New Orleans, LA, USA, Apr./May 2004, pp. 4393–4398.

[37] N. Michael, D. Mellinger, Q. Lindsey, and V. Kumar, "The GRASP multiple micro-UAV testbed," *IEEE Robot. Autom. Mag.*, vol. 17, no. 3, pp. 56–65, Sep. 2010.

[38] Institute for Visual Computing, Swiss Federal Institute of Technology in Zürich. (2014). *QGroundControl*. [Online]. Available: http://www.qgroundcontrol.org/, accessed Jul. 13, 2014.

[39] G. Fink, "Visual servoing and nonlinear control of unmanned aerial vehicles," Ph.D. Candidacy Report, Dept. Elect. Comput. Eng., Univ. Alberta, Edmonton, AB, Canada, 2015.

[40] T. Dierks and S. Jagannathan, "Output feedback control of a quadrotor UAV using neural networks," *IEEE Trans. Neural Netw.*, vol. 21, no. 1, pp. 50–66, Jan. 2010.

[41] R. C. Leishman, J. C. Macdonald, R. W. Beard, and T. W. McLain, "Quadrotors and accelerometers: State estimation with an improved dynamic model," *IEEE Control Syst.*, vol. 34, no. 1, pp. 28–41, Feb. 2014.

[42] K. Alexis, G. Nikolakopoulos, and A. Tzes, "Constrained-control of a quadrotor helicopter for trajectory tracking under wind-gust disturbances," in *Proc. 15th IEEE Medit. Electrotech. Conf.*, Valletta, Malta, Apr. 2010, pp. 1411–1416.